Ann. Geophys., 27, 2361–2369, 2009
www.ann-geophys.net/27/2361/2009/

Annales Geophysicae

Gravity wave amplitudes and momentum fluxes inferred from OH airglow intensities and meteor radar winds during SpreadFEx

F. Vargas[1], **D. Gobbi**[1], **H. Takahashi**[1], **and L. M. Lima**[2]

[1]Instituto Nacional de Pesquisas Espaciais (INPE), São José dos Campos, Brazil
[2]Universidade Estadual da Paraíba (UEPB), Campina Grande, PB, Brazil

Received: 7 May 2008 – Revised: 23 February 2009 – Accepted: 26 February 2009 – Published: 8 June 2009

Abstract. We show in this report the momentum flux content input in the mesosphere due to relatively fast and small scale gravity waves (GWs) observed through OH airglow images. The acquisition of OH NIR images was carried out in Brazil at Brasilia (14.8° S, 47.6° W) and Cariri (7.4° S, 36.5° W) from September 2005 to November 2005 during the SpreadFEx Campaign. Horizontal wind information from meteor radar was available in Cariri only. Our findings showed strong wave activity in both sites, mainly in Cariri. High wave directionality was also observed in both sites during SpreadFEx, which have been observed by other investigators using different analysis' techniques and different types of data during the campaign. We discuss also the possibility of plasma bubble seeding by gravity waves presenting spatial and temporal scales estimated with our novel analysis technique during the SpreadFEx campaign.

Keywords. Atmospheric composition and structure (Airglow and aurora) – Meteorology and atmospheric dynamics (Middle atmosphere dynamics; Waves and tides)

1 Introduction

Atmospheric gravity waves have a great significance in the global circulation at mesosphere and lower thermosphere (MLT) region. In this sense, there is considerable interest in measuring momentum fluxes carried by those waves (Holton, 1982; Gardner et al., 1999). Co-located optical imagers and radar wind instruments (mean horizontal wind information) at the same observation site are combined to provide intrinsic wave parameters (frequency, horizontal wavelength, direction of propagation), determined directly from the airglow images. Intrinsic wave parameters permit to estimate the momentum fluxes, which are used as indicators of wave activities at the mesosphere region (e.g., Swenson and Liu, 1998). The vertical wavelength is calculated from the theory of the gravity wave propagation as usual by using the dispersion relation. The gravity wave amplitude is another essential parameter required to infer wave fluxes.

The task of determining wave amplitudes by way of airglow variations is not simple, mainly for two reasons: first, the altitude variation of the minor constituent perturbations are not the same of that the background gas, i.e. the airglow chemistry generally is important; second, the wave amplitude is related to the vertical extension of the airglow emission layer (∼8 km), which filters out short vertical wavelength gravity waves. Swenson and Liu (1998) and Vargas et al. (2007) have developed a method of representing analytically perturbations of the airglow emission radiance (ratio between the radiance I and temperature T variances) as a means of estimating wave momentum fluxes from all-sky airglow image data. Specifically for the OH emission, the ratio $(I'/I)/(T'/T)$, called the "Cancellation Factor", CF, is approximated by the exponential fitting (Vargas et al., 2007)

$$\mathrm{CF} = 3.68 - 3.41\exp[-0.0053(\lambda_z - 6)^2] \quad (1)$$

where the vertical wavelength λ_z is given in km (CF can be neglected if $\lambda_z < 6$ km). Virtually the equation is not valid for vertical wavelengths smaller than 12 km because the error associated with CF is very large in this range.

In this study, the momentum flux per mass unit is defined as the covariance between the horizontal (u', v') and vertical (w') wind fluctuations, averaged over one wave cycle. Here u' is the fluctuation on the zonal wind and v' is the fluctuation on the meridional wind. Zonal and meridional components of wave fluxes are calculated by using the acoustic-gravity wave polarization relations in terms of the temperature amplitudes (Fritts and Alexander, 2003) and CF model (Eq. 1),

Correspondence to: F. Vargas
(fabio.vargas.br@gmail.com)

Published by Copernicus Publications on behalf of the European Geosciences Union.

that are combined to give a set of equations for zonal and meridional momentum flux, that is:

$$F_{\mathrm{Zon}}/\bar{\rho} = \langle u'w' \rangle = -\frac{1}{2}\frac{km\omega^2}{k^2+l^2}\frac{g^2}{N^4}\left(\frac{I'/\bar{I}}{\mathrm{CF}}\right)^2$$
$$F_{\mathrm{Mer}}/\bar{\rho} = \langle v'w' \rangle = -\frac{1}{2}\frac{lm\omega^2}{k^2+l^2}\frac{g^2}{N^4}\left(\frac{I'/\bar{I}}{\mathrm{CF}}\right)^2 \quad (2)$$

where $\bar{\rho}$ is the mean mass density of the atmosphere, k and l are the zonal and meridional wavenumbers, m is the vertical wavenumber, ω is the intrinsic frequency, g is the gravity acceleration and N the buoyancy frequency.

Image data obtained during the SpreadFEx campaign at two sites, Brasilia (14.8° S, 47.6° W) and Cariri (7.4° S, 36.5° W) with optical imagers of OH NIR airglow are used for gravity wave studies. Particularly for Cariri, these measures are combined with radar wind observations to infer intrinsic wave parameters. General characteristics of gravity wave parameters obtained and momentum fluxes estimations were investigated in this paper. A short discussion in terms of momentum fluxes is presented for two nights with evidence of strong correlation between wave motion followed by ionospheric plasma depletion, which are compared to the results obtained by Takahashi et al. (2009).

2 Observations and data analysis

The database used in this report has been taken at two sites in Brazil during the SpreadFEx Campaign by using two all-sky airglow imagers. Both of them use a backilluminated CCD sensor of 1024×1024 pixels. The exposition time was 15 s for recording OH images, while the sampling rate between images was about 2 min. An all-sky CCD image covers a large horizontal extension of the nocturnal sky, but here it was used an area of 512×512 km centered at the zenith in order to avoid lens distortion at the edges of the images. For a complete description of the all-sky CCD imagers used in this work see Takahashi et al. (2009) or Medeiros et al. (2004).

We selected for analysis 15 nights of OH images in Brasilia and 21 nights of data in Cariri. Time intervals of clear nocturnal sky of each night were selected by using keogram analysis. Keograms are built from the images acquired during the night by taking the central row (or column) of each one and placing them side by side in a new image. Keograms permit to check rapidly the luminosity of the central portion of the sky during the observation period and also permit to define quickly the best time interval for analysis during one specific night.

During the campaign in Cariri, horizontal wind data obtained with meteor radar were available, but not in Brasília. Horizontal wind estimation over Brasilia for one single night (from 24 October to 25 October) was provided by S. Vadas (private communication). S. Vadas used meteor radar wind data (averaged) from 80–100 km linearly interpolated to the TIME-GCM (thermosphere – ionosphere – mesosphere – electrodynamics general circulation model) to estimate horizontal wind magnitudes over Brasilia. We used those wind profiles ahead in this paper for pointing out differences observed on the estimated wave parameters under the influence of the horizontal atmospheric flow.

Gravity waves present in airglow images were analyzed with a modified version of the method described by Tang et al. (2005). Their analysis method was designed for obtaining wave parameters (frequency, horizontal and vertical wavelength, phase velocity, propagation direction, relative wave amplitude I'/I) and associated energy and momentum fluxes of GWs disturbing the OH layer only. We have extended the method by including O_2 and OI5577 emissions. We will give here only general aspects of the extended version of Tang's method. A complete description of it will be given in a separate paper.

The field of view considered in our procedure has an extension of 512×512 km. It was defined a box of 150×150 km of field of view for analysis and GW parameter estimation. We can avoid spectral contamination of the Milky Way if it is appearing on the images by changing the position of the analysis box by placing it at the southeast portion of the image. The analysis box is positioned at the zenith of the image when it is not the case.

The algorithm performs first typical corrections on the images, including flat fielding, unwarping and star removal operations. If horizontal wind information is available, it is used for Doppler shift correction of each image (Fig. 1a). The images acquired during one specific night are then subtracted from one to another to obtain time difference (TD) images (Fig. 1b). The time difference operation benefits the detection of small period waves (high frequency), working as a bandpass filter of large wave periods. Also, TD images show a better contrast, which benefits visual inspection of waves on the field of view. The amount of images recorded in one night depends on the observational conditions during that period. Typically more than 200 images of the OH emission are recorded during one observation night.

The method processes a set of three sequential images which result in two TD images and automatically calculates wave parameters of prominent events in the field of view (Fig. 1b). At this point, the cross spectra is computed by using two remaining TD images. The amplitude periodogram is a result of the cross spectra operation (Fig. 1c) and is used for estimating the relative amplitude I'/I of dominant waves (prominent peaks), their direction of propagation and their horizontal wavelength. Basically, the direction of propagation is given by the position of the peak in the plot in terms of wavelength (cartesian relation between the x-component of the position and the y-component). The relative amplitude I'/I is given by the integrated area surrounding a prominent peak. The horizontal wavelength is the distance from the origin of periodogram to that given peak. The phase velocity and the period of dominant waves are obtained from the

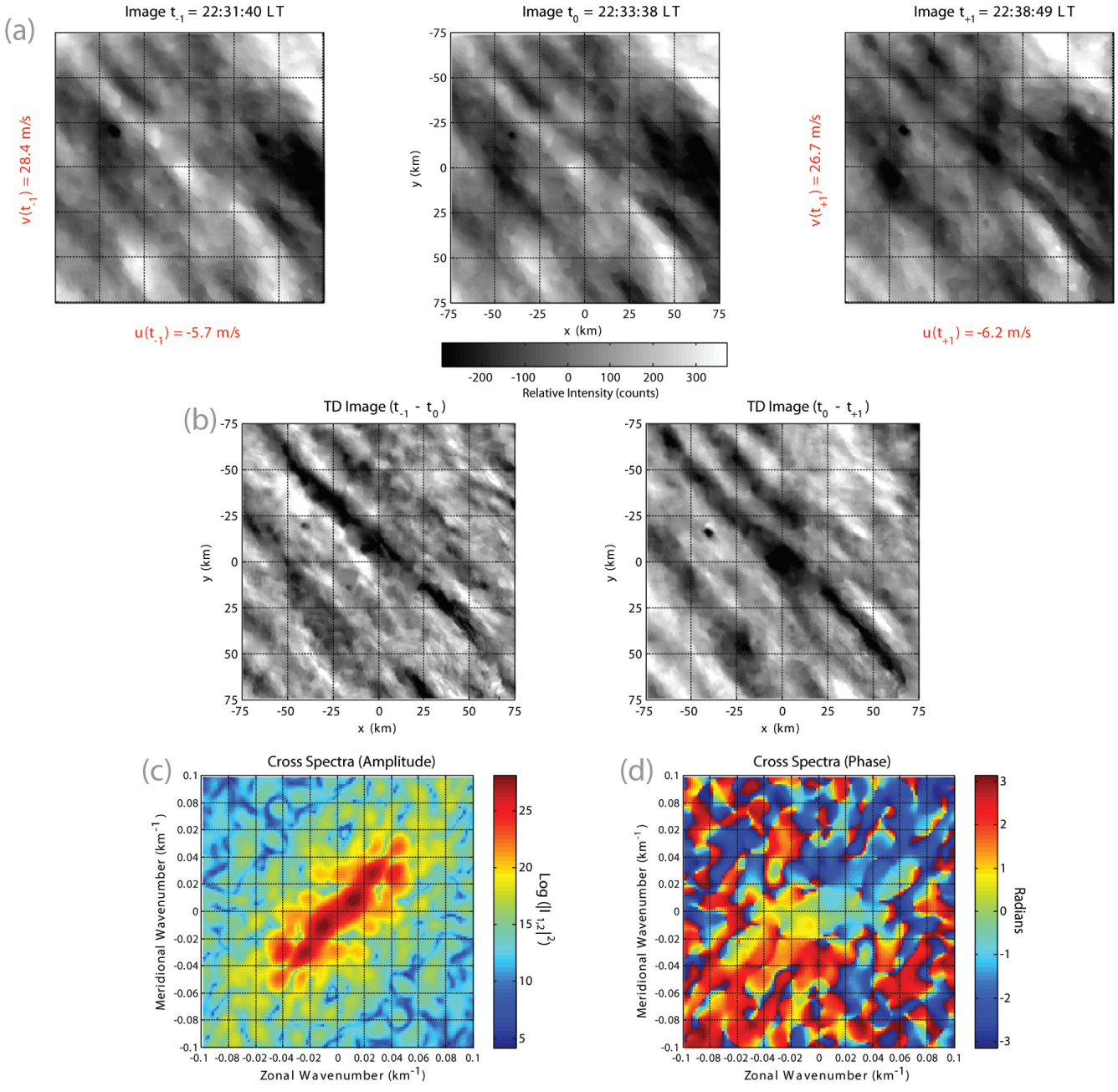

Fig. 1. Processing of a set of three airglow images in order to obtain the cross spectra. In **(a)** it is showed a set of sequential OH images presenting GW structures. **(b)** Time difference images obtained from the set of images. **(c)** Amplitude cross-spectra of the TD images, from where we estimate the wave amplitude, propagation direction and horizontal wavelength. **(d)** Phase cross-spectra of the TD images showed in (a).

phase periodogram (Fig. 1d). If wind information is available in the course of GW events we estimate intrinsic phase velocity and period of waves.

Because we are using TD images, we have to correct the wave amplitude before calculating the momentum flux. The correction of the relative wave amplitude is done properly in our analysis procedure. Relative wave amplitudes obtained from TD images depend on their intrinsic frequency and the sampling rate of images. Small period waves, in general, have their amplitude reinforced due to wave superposition, while large period waves have its amplitude reduced, that is, TD operation works as a bandpass filter. Small period waves carry large energy and are in the range of periods where optical imagers are more sensitive to detection (Swenson and Liu, 1988; Swenson et al., 1999).

Table 1. Momentum flux (F_M) and propagation direction (θ) of gravity waves observed in Cariri and Brasilia. The standard deviation of each parameter is also showed in the table. The label "#" refers to the number of GW events detected by the analysis method. Prefixes "zen" and "off" refer to the analysis performed at zenith and off-zenith of the image, respectively.

Brasilia				Cariri			
Day (yymmdd)	#	$F_M \pm \sigma$ ($m^2 s^2$)	$\theta \pm \sigma$ (degree)	Day (yymmdd)	#	$F_M \pm \sigma$ ($m^2 s^2$)	$\theta \pm \sigma$ (degree)
				zen_050923	2	3.1±2.5	303±0
off_050924	2	14.2±12.4	198±220	off_050924	7	1.9±1.0	43±7
				zen_050925	16	7.3±21.5	268±128
				zen_050928	21	8.1±12.4	178±132
zen_050929	11	5.3±4.6	221±99	zen_050929	17	14.5±19.2	232±129
zen_050930	91	8.1±11.8	95±130	zen_050930	10	13.8±24.7	166±152
zen_051001	49	5.7±8.1	296±130	zen_051001	31	7.4±9.6	124±131
off_051002	25	8.5±12.8	132±103				
zen_051003	57	5.1±12.5	89±59	zen_051003	17	10.5±19.7	254±94
				zen_051005	67	14.0±22.7	234±83
zen_051006	24	7.7±16.5	230±83	zen_051006	18	18.4±21.8	252±84
zen_051007	157	4.9±9.7	220±146				
zen_051008	95	4.4±10.2	40±77	zen_051008	7	16.0±16.5	126±102
				zen_051009	20	11.1±18.5	198±139
zen_051022	27	4.7±9.3	155±134				
zen_051023	17	15.2±22.6	271±92				
zen_051024	9	3.9±3.1	173±95				
zen_051025	44	7.5±14.0	274±107				
zen_051026	44	9.6±10.8	168±51	zen_051026	9	9.8±8.0	138±79
zen_051027	30	11.8±19.9	173±157	off_051027	1	8.6	147
				zen_051028	29	10.2±13.4	213±102
				zen_051029	31	7.5±17.2	209±153
				zen_051030	6	2.5±1.8	41±6
				zen_051031	7	9.1±14.9	279±28
				zen_051101	7	4.9±4.7	158±161
				zen_051102	19	12.0±24.4	272±52
				zen_051103	19	15.7±18.0	225±82
				zen_051104	51	8.1±11.6	221±121
zen_051106	56	6.3±12.7	195±139				

Typical gravity wave parameters were obtained from the analysis of several images acquired in Brazil by using our analysis technique. In this work, the following values of wave parameter were found: horizontal wavelength ranged from 10 to 150 km, vertical wavelength from ∼6 to 40 km and periods of ∼6 to 60 min; phase velocities ranged from 50 to 150 m/s (corresponding to relatively fast waves). The vertical wavelength is calculated by using the dispersion relation of GWs. Similar values of wave parameters have been observed at different sites by other investigators using airglow images (e.g., Pautet et al., 2005).

It was performed the momentum flux estimation of each wave event detected by the analysis procedure after processing the images. Because the waves are identified by following their horizontal direction of propagation, the equations for zonal and meridional flux are combined to give rise to one equation for the momentum flux toward the direction of propagation of the wave (Swenson and Liu, 1998; Swenson et al., 1999; Liu and Swenson, 2003; Vargas et al., 2007):

$$F_M/\bar{\rho} = -\frac{1}{2}\frac{g^2}{N^4}\frac{\omega^2 m}{k_h}\left(\frac{I'/I}{\mathrm{CF}}\right)^2 \quad (3)$$

where $k_h=(k^2+l^2)^{0.5}$ is the horizontal wavenumber.

Vargas et al. (2007) have modeled CF for three mesospheric airglow layers (OH, O_2 and OI5577), which allows us to compute the momentum flux of GWs in three different layers. In addition, if the same wave is observed simultaneously in two layers, the model developed in Vargas et al. (2007) allows calculating the wave forcing $-\bar{\rho}^{-1}\partial F_M/\partial z$ on the atmosphere by using Eq. (3) for each emission layer. Estimative of GW forcing on the mesosphere during the SpreadFEx campaign was not possible because lack of images of O_2 and OI5577 emission in both observation sites. However, a paper is being prepared for showing results about GW forcing by using a large database of images and wind profiles obtained in two sites in Brazil during four years of observations.

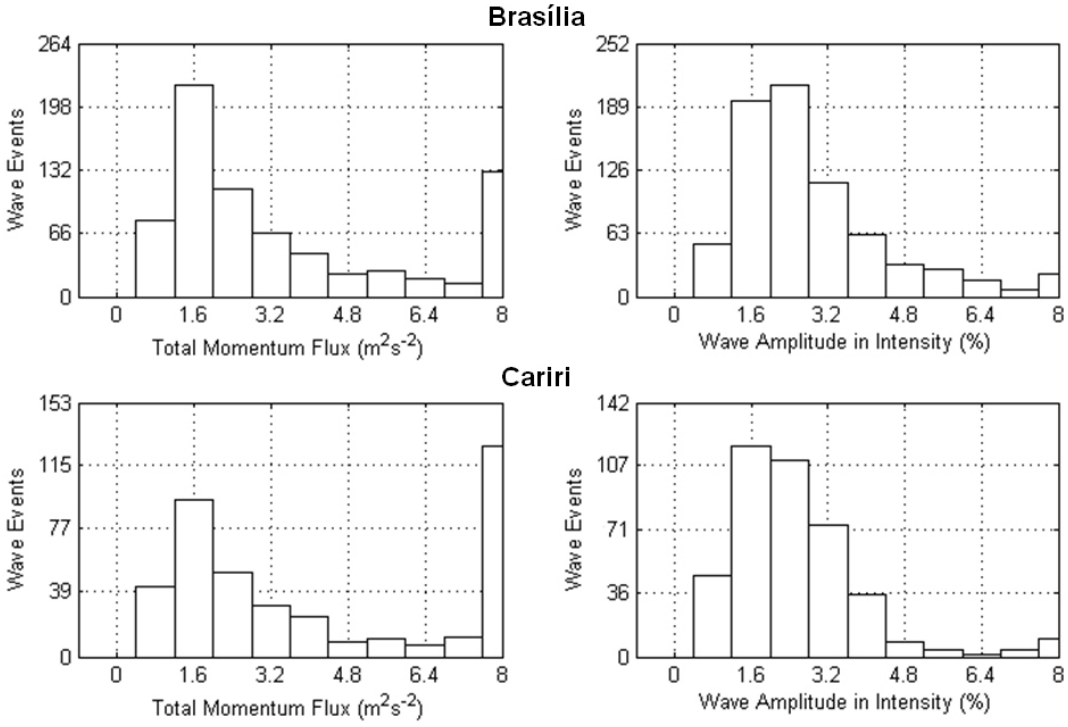

Fig. 2. Histograms of momentum flux and relative wave amplitude distributions in both sites, Cariri and Brasilia.

Table 2. Averaged values of gravity wave parameters (horizontal wavelength, λ_x; vertical wavelength, λ_z; period, τ; and phase velocity, c) obtained for each site. In Cariri the averaged values represent intrinsic characteristics of GWs (subscript i), while in Brasilia the obtained parameters are extrinsic due to lack of horizontal wind information.

Brasília				Cariri			
λ_x (km)	λ_z (km)	τ (min)	c (m/s)	λ_x (km)	λ_z (km)	τ_i (min)	c_i (m/s)
59±30	27±33	17±9	64±31	84±23	28±44	26±13	94±138

3 Momentum flux of gravity waves

The analysis procedure described here was applied in several images taken with CCD all-sky imagers located at Cariri and Brasilia during SpreadFEx. Overall estimatives of momentum fluxes pointed out strong wave activity in both sites.

Table 1 shows the nocturnal average of momentum flux in Brasilia and Cariri. It shows also the standard deviation of F_M, the averaged propagation direction θ (θ=0 at east, positive counterclockwise) and the standard deviation of events detected by the analysis procedure. Standard deviations act as indicators of variability of the wave field. The column labeled "#" indicates the number of events detected in a given night. It was available 9 days of coincident airglow data for both sites. In the column labeled "Day", the prefix "zen" indicates that the analysis window was located at zenith of the image, while the prefix "off" indicates the window positioned at the southeast sector of the image (off zenith) for avoiding spectral contamination from the Milky Way.

The strongest GW flux in Brasilia occurred on 23 October, when the average momentum flux was $\sim$15 m^2 s^{-2}, with a high variability indicated by the standard deviation for this night ($\pm$23 m^2 s^{-2}). We observed strong preference for southeastward propagation during that night, with θ=270±90 degrees. The standard deviation of θ suggests large anisotropy of the wave field during the observation time. Directional GW field also occurred on 26 October (θ=168±50 degrees), when the waves moved preferentially westward. Overall estimative showed that the mean value of momentum flux during the whole campaign was of 6.5±12.1 m^2 s^{-2} in Brasilia, while the mean wave amplitude in radiance was of 2.9±1.9% at the same site, which is a significant disturbance on the OH layer (e.g., Tang et al., 2005).

The situation was a bit different in Cariri. On 6 October, the largest value of momentum flux (18.4±21.8 m^2 s^{-2}) and also high directionality of the wave field (θ=252±84 degrees) was observed. Eighteen wave events were detected during that night. In Cariri, the mean value of the momentum

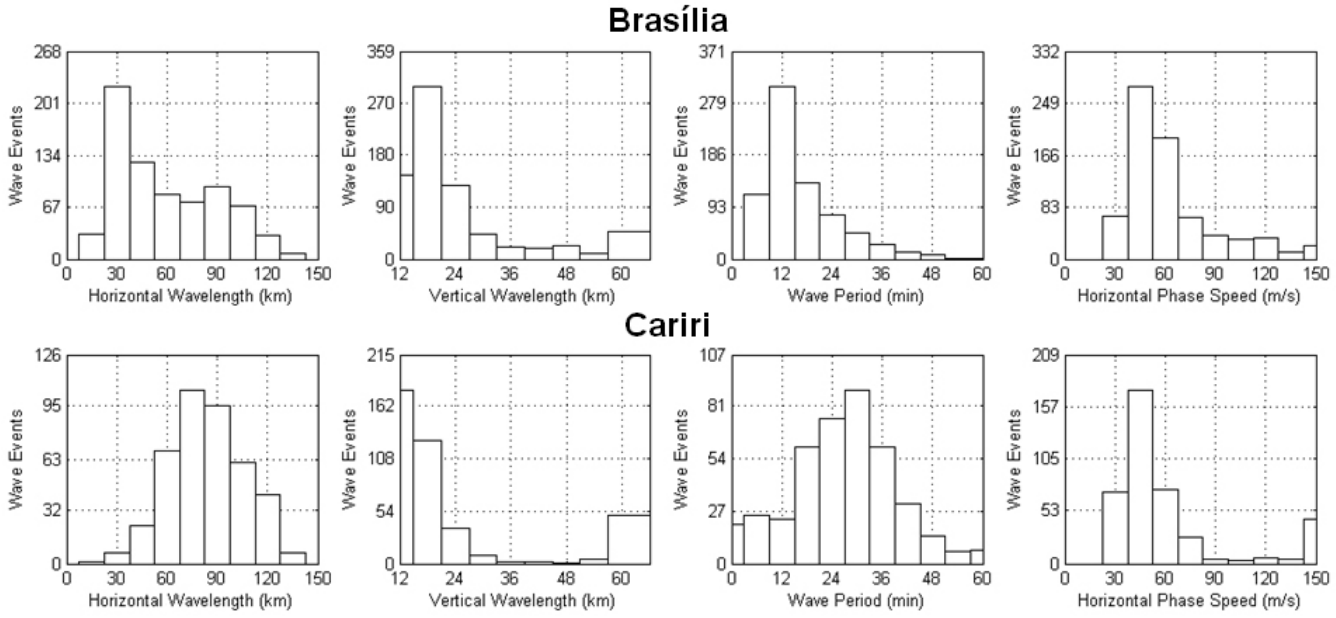

Fig. 3. Histograms of gravity wave parameter distributions in both sites, Brasilia and Cariri. In Brasilia the parameter are observable quantities (extrinsic), while in Cariri the parameters are intrinsic.

flux was of $10.7 \pm 17.5\,m^2\,s^{-2}$ (larger than in Brasilia) and the mean wave amplitude was of $2.7 \pm 2.3\%$. Observe that by wave event we mean a single peak present on the magnitude periodogram obtained from one set of TD images (Fig. 1c). If a wave is found in the next image set, we consider it as a different wave happening during that time interval.

Figure 2 shows histograms of the distribution of momentum flux and wave amplitude versus number of wave events. The shape of momentum flux distributions are similar in both sites, which are mainly due to the quadratic dependence of the momentum flux to the wave amplitude (see Eq. 3). Once we lack horizontal wind information in Brasilia, it seems that the Doppler shift did not have a strong influence on the momentum flux distribution.

We also analysed GW parameters estimated during the campaign. Figure 3 shows histograms of observed horizontal and vertical wavelengths, wave period and phase velocity for events observed in Brasilia and Cariri. Horizontal wavelength histograms exhibit distinct peaks: 30 km and 80 km, respectively. The same is found for the wave period distribution: 12 min and 30 min, respectively. Table 2 presents averaged values of four different parameters determined during the SpreadFEx campaign. These averaged values confirm the shape of their related distributions in each site. A more realistic comparison of wave parameters in different sites would be possible if the Doppler shift correction were performed on the images in order to obtain the intrinsic wavelengths and periods in Brasilia.

For clarifying the influence of the horizontal wind on the gravity wave parameters, we compare the results of our analysis procedure for one night in Brasilia. First the airglow data was processed including no wind data in the algorithm. Modeled horizontal wind profiles provided by S. Vadas were used during the night of 24 October for obtain intrinsic wave parameters. Modeled wind profiles will not reproduce actual conditions of the atmosphere in which GWs are propagating. They were used here just to point out differences in wave parameters when wind data is not present. The outputs of the algorithm are showed in Fig. 4. The angular plots of horizontal wind direction are showed on the panels (a) and (d). The angular distributions of momentum flux versus direction of propagation of each wave event during the night are showed in the panels (b) and (e). The phase velocity versus horizontal wavelength are given on the panels (c) and (f).

The region in between the thick lines in the phase velocity versus horizontal wavelength charts indicates a region of vertical propagating waves (Fig. 4c and f). Many propagating events can be seen during the night of 24 October. The bottom thick line indicates a cutoff, where the analysis method is not sensitive enough for detecting events. Below that limit (vertical wavelength smaller than $\sim$12 km), the error associated to the cancellation factor is very large (see Eq. 1) and estimative of the momentum flux is not realistic. The region above the top thick line indicates a region of evanescent waves, where vertical wavelengths of waves are too large and probably the waves do not propagate upward. For better comprehension of those limits, the reader is referred to the work of Swenson et al. (2000). We did not observe any evanescent waves or waves close to the evanescent limit for that night, even when wind information was considered in the analysis.

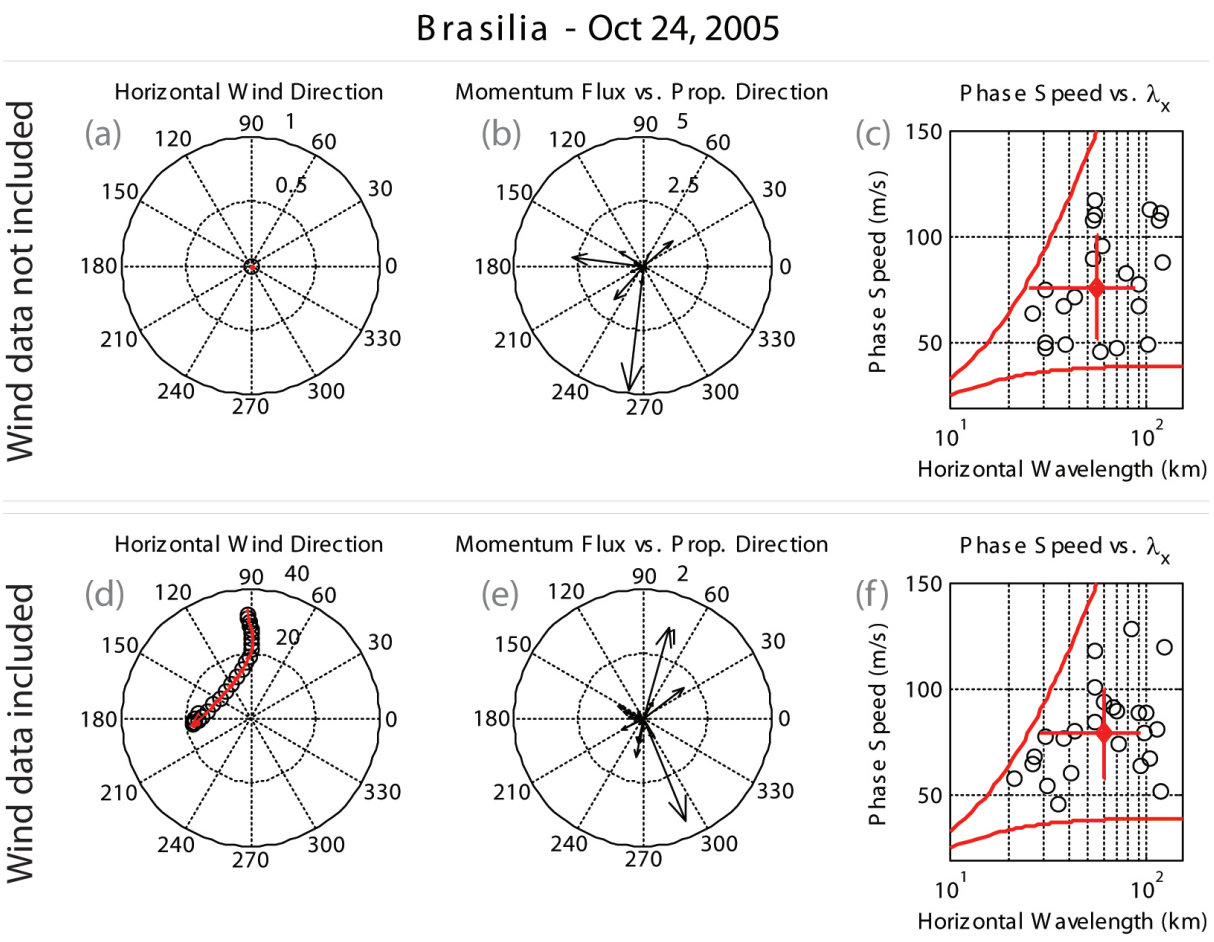

Fig. 4. Differences of wave parameters (night of 24 October, Brasilia) in two different situations: wind information is considered or not considered in the analysis procedure. Panels **(a)** and **(d)** show angular plot of wind data available for the night. Panels **(b)** and **(e)** show the angular distribution of the direction of propagation and the momentum flux magnitude of detected wave events. Panels **(c)** and **(f)** show the distribution of wave events in face to their phase velocities and horizontal wavelength. Thick red lines indicate the limits of the analysis procedure for detection of gravity waves.

Figure 4b and e suggests a wave field that propagates to the opposite direction of the horizontal wind, which is consistent with the wind filtering theory (e.g. McLandress, 1998; Espy et al., 2004). While the modeled horizontal wind is northwest oriented, the flux of waves points in the opposite direction, which indicates wave blocking in that direction. It is evident the importance of including wind information in our analysis once it were observed obvious changes in wave directions and momentum flux magnitudes, as can be seen in the central charts of Fig. 4. However, the modeled wind used here gives only a crude idea of the mesospheric conditions during the observation period. Actual wind information has to be taken into account if a realistic estimative of the momentum flux is necessary.

4 Summary

In this work, we have focused on demonstrating spatial and temporal scales of GWs detected in OH NIR images and their associated amplitudes and momentum fluxes during SpreadFEx campaign. Part of the events observed using the analysis technique presented here fits into the range of waves that can easily penetrate into higher altitudes reaching the botton of the ionospheric F-region. Temporal and spatial scales of waves that can penetrate higher into the atmosphere are given in Vadas and Fritts (2004) and range from 30 to 50 km of vertical wavelength, 80 to 130 km of horizontal wavelength and 70 to 120 m/s of horizontal phase velocities ($\omega \sim N/3$). Some observed wave amplitudes that were found large enough for disturbing the bottomside of the ionospheric region and possibly could give rise to Rayleigh-Taylor instabilities and plasma bubbles. However, GW penetration still depends on propitious atmospheric conditions, that is, the

absence of filtering of GWs by tidal or larger scale winds and absence of turning levels between mesosphere and ionospheric F-layer.

Takahashi et al. (2009) have successfully investigated some cases of strong correlation between GWs motion in the mesosphere followed by plasma bubble appearing above in the F-region at Cariri. Because we had access to the same database as Takahashi et al. (2009), it was possible to estimate the momentum flux and wave amplitudes at the same time intervals of those waves cited in their report. For that comparison we used wind information, once it was available in Cariri during the campaign.

Takahashi et al. (2009) have observed large horizontal scale waves from 23:00 to 24:00 UT during the evening of 30 September in that observation site. Our analysis has identified a group of large scale GWs getting into the field of view during that same time interval too. Estimative of horizontal wavelength of those events using our method ranged from 90 to 130 km. Vertical wavelengths of those GWs ranged from 22 to 65 km and their intrinsic periods ranged from 11 to 25 min. The propagation direction of those GW events were also consistent with those pointed out by the investigators (toward southeast quadrant). Takahashi et al. (2009) have also studied waves during 1 October evening from 22:00 to 25:00 UT. We have found at that time a train of waves presenting large horizontal wavelength (111 km in average), vertical and temporal scales of 40 km and 18 min, respectively. The directions of propagation were found compatible with a preferential motion eastward.

Our estimations of the momentum flux during those time intervals were not larger than $0.7\,m^2\,s^{-2}$ on 30 September, and not larger than $1.7\,m^2\,s^{-2}$ on 1 October. These values do not represent a significant quantity of momentum flux if compared to the stronger wave events observed during the campaign. Stronger momentum flux events can reach magnitudes of more than $5\,m^2\,s^{-2}$. Also the wave parameters of those events suggest that they are not likely to reach the bottom of the ionosphere layer (Fritts and Alexander, 2003). However, the timing between wave events and plasma bubble occurrence is significant, which could suggest a plasma bubble event being triggered by one of those wave events.

Other assessments of gravity wave parameters have been made by Taylor et al. (2009) during SpreadFEx, while Vadas et al. (2009) have performed calculations of momentum fluxes, amplitudes and wave parameters for monochromatic GW events during the campaign. Their method was based in estimate GW properties of individual and prominent wave events present in the airglow images. Momentum fluxes were computed assuming a Krassovsky ratio $|\eta|$=3. It was used the modeled CF parameter instead of the Krassovsky ratio in our analysis method in order to give an estimate of wave perturbation in atmospheric temperature (not temperature weighted by the volume emission rate) in terms of spectral airglow radiance (Vargas et al., 2007).

Vadas et al. (2009) showed waves presenting momentum fluxes ranging from 1 to $10\,m^2\,s^{-2}$, which are perfectly compatible with the findings presented in this paper. We also found agreement among wave amplitudes identified here with those presented by Vadas et al. (2009). While they have focused in prevalent waves occurring at airglow altitudes, our method is able to identify any vertical propagating event appearing over the field of view of the all-sky imager. We believe that the analysis procedure used here was able to give a more complete assessment of relatively fast, small scale waves in regime of vertical propagation and their associated quantities during the SpreadFEx campaign.

Acknowledgements. The authors are deeply grateful to Sharon Vadas for providing interpolated wind information for Brasilia. Thanks to Dominique Pautet for his help in preprocessing of Brasilia images. We are also grateful to Dave Fritts for encouraging us during the preparation of this report.

Topical Editor U.-P. Hoppe thanks two anonymous referees for their help in evaluating this paper.

References

Espy, P. J., Jones, G. O. L., Swenson, G. R., Tang, J., and Taylor, M. J.: Tidal modulation of the gravity-wave momentum flux inthe Antarctic mesosphere, Geophys. Res. Lett., 31, L11111, doi:10.1029/2004GL019624, 2004.

Fritts, D. C. and Alexander, M. J.: Gravity wave dynamics and effects in the middle atmosphere, Rev. Geophys., 41(1), 1003, doi:10.1029/2001RG000106, 2003.

Fritts, D. C., Abdu, M. A., Batista, B. R., Batista, I. S., Batista, P. P., Buriti, R., Clemesha, B. R., Dautermann, T., de Paula, E. R., Fechine, B. J., Fejer, B. G., Gobbi, D., Haase, J., Kamalabadi, F., Kherani, E. A., Laughman, B., Lima, P. P., Liu, H.-L., Medeiros, A., Pautet, P.-D., Riggin, D. M., Rodrigues, F. S., São Sabbas, F., Sobral, J. H. A., Stamus, P., Takahashi, H., Taylor, M. J., Vadas, S. L., Vargas, F., and Wrasse, C. M.: Overview and summary of the Spread F Experiment (SpreadFEx), Ann. Geophys., 27, 2141–2155, 2009, http://www.ann-geophys.net/27/2141/2009/.

Gardner, C. S., Gulati, K., Zhao, Y. C., and Swenson, G.: Measuring gravity wave momentum fluxes with airglow imagers, J. Geophys. Res.-Atmos., 104(D10), 11903–11915, 1999.

Holton, J. R.: The role of gravity wave induced drag and diffusion in the momentum budget of the mesosphere, J. Atmos. Sci., 39, 791–799, 1982.

Liu, A. Z. and Swenson, G. R.: A modeling study of O-2 and OH airglow perturbations induced by atmospheric gravity waves, J. Geophys. Res.-Atmos., 108(D4), 4151, doi:10.1029/2002JD002474, 2003.

McLandress, C.: On the importance of gravity waves in the middle atmosphere and their parameterization in general circulation models, J. Atmos. Solar-Terr. Phys., 60, 1357–1383, 1998.

Medeiros, A. F., Buriti, R. A., Machado, E. A., Takahashi, H., Batista, P. P., Gobbi, D., and Taylor, M. J.: Comparison of gravity wave activity observed by airglow imaging at two different latitudes in Brazil, J. Atmos. Sol.-Terr. Phys., 66(6–9), 647–654, 2004.

Pautet, P.-D., Taylor, M. J., Liu, A. Z., and Swenson, G. R.: Climatology of short-period gravity waves observed over northern Australia during the Darwin Area Wave Experiment (DAWEX) and their dominant source regions, J. Geophys. Res., 110, D03S90, doi:10.1029/2004JD004954, 2005.

Swenson, G. R. and Liu, A. Z.: A model for calculating Acoustic Gravity Wave energy and momentum flux in the mesosphere from OH airglow, Geophys. Res. Lett., 25(4), 477–480, doi:10.1029/98GL00132, 1998.

Swenson, G. R. and Gardner, C. S.: Analytical models for the responses of the mesospheric OH* and Na layers to atmospheric gravity waves, J. Geophys. Res.-Atmos., 103(D6), 6271–6294, 1998.

Swenson, G. R., Liu, A. Z., Li, F., and Tang, J.: High frequency atmospheric gravity wave damping in the mesosphere, Adv. Space Res., 32(5), 785–793, 2003.

Swenson, G. R., Haque, R., Yang, W., and Gardner, C. S.: Momentum and energy fluxes of monochromatic gravity waves observed by an OH imager at Starfire Optical Range, New Mexico, J. Geophys. Res.-Atmos., 104(D6), 6067–6080, 1999.

Takahashi, H., Taylor, M. J., Pautet, P.-D., Medeiros, A. F., Gobbi, D., Wrasse, C. M., Fechine, J., Abdu, M. A., Batista, I. S., Paula, E., Sobral, J. H. A., Arruda, D., Vadas, S. L., Sabbas, F. S., and Fritts, D. C.: Simultaneous observation of ionospheric plasma bubbles and mesospheric gravity waves during the SpreadFEx Campaign, Ann. Geophys., 27, 1477–1487, 2009, http://www.ann-geophys.net/27/1477/2009/.

Tang, J., Kamalabadi, F., Franke, S. J., Liu, A. Z., and Swenson, G. R.: Estimation of gravity wave momentum flux with spectroscopic imaging, IEEE Trans. Geosci. Remote Sens., 43(1), 103–109, 2005.

Taylor, M. J., Pautet, P.-D., Medeiros, A. F., Buriti, R., Fechine, J., Fritts, D. C., Vadas, S. L., Takahashi, H., and São Sabbas, F. T.: Characteristics of mesospheric gravity waves near the magnetic equator, Brazil, during the SpreadFEx campaign, Ann. Geophys., 27, 461–472, 2009, http://www.ann-geophys.net/27/461/2009/.

Vadas, S. L., Fritts, D. C., Pautet, P.-D., Taylor, M. J., Liu, H.-L., Batista, P. P., Takahashi, H., Sao Sabbas, F., Stamus, P., Medeiros, A. F., Buriti, R., and Fechine, J.: Amplitudes, scales, and variability of gravity waves in the thermosphere from convective plumes over Brazil, Ann. Geophys., to be submitted, 2009.

Vadas, S. L. and Fritts, D. C.: Thermospheric responses to gravity waves arising from mesoscale convective complexes, J. Atmos. Solar-Terr. Phys., 66, 781–804, 2004.

Vargas, F., Swenson, G., Liu, A., and Gobbi, D.: O(^{1}S), OH, and O_2(b) airglow layer perturbations due to AGWs, and their implied effects on the atmosphere., J. Geophys. Res., 112, D14102, doi:10.1029/2006JD007642, 2007.